HAL
open science

Reaction of Ni film with In0.53Ga0.47As: Phase formation and texture

Seifeddine Zhiou, Thanh Tra Nguyen, Philippe Rodriguez, Fabrice Nemouchi, Laetitia Rapenne, Nils Blanc, Nathalie Boudet, Patrice Gergaud

To cite this version:

Seifeddine Zhiou, Thanh Tra Nguyen, Philippe Rodriguez, Fabrice Nemouchi, Laetitia Rapenne, et al.. Reaction of Ni film with In0.53Ga0.47As: Phase formation and texture. Journal of Applied Physics, 2016, 120 (13), pp.135304. 10.1063/1.4963716 . cea-01559846

HAL Id: cea-01559846

https://cea.hal.science/cea-01559846

Submitted on 11 Jul 2017

HAL is a multi-disciplinary open access archive for the deposit and dissemination of scientific research documents, whether they are published or not. The documents may come from teaching and research institutions in France or abroad, or from public or private research centers.

L'archive ouverte pluridisciplinaire **HAL**, est destinée au dépôt et à la diffusion de documents scientifiques de niveau recherche, publiés ou non, émanant des établissements d'enseignement et de recherche français ou étrangers, des laboratoires publics ou privés.

AIP Journal of Applied Physics

Reaction of Ni film with In0.53Ga0.47As: Phase formation and texture

Seifeddine Zhiou, Tra Nguyen-Thanh, Philippe Rodriguez, Fabrice Nemouchi, Laetitia Rapenne, Nils Blanc, Nathalie Boudet, and Patrice Gergaud

Citation: Journal of Applied Physics **120**, 135304 (2016); doi: 10.1063/1.4963716
View online: http://dx.doi.org/10.1063/1.4963716
View Table of Contents: http://scitation.aip.org/content/aip/journal/jap/120/13?ver=pdfcov
Published by the AIP Publishing

Articles you may be interested in

Epitaxial NiInGaAs formed by solid state reaction on In0.53Ga0.47As: Structural and chemical study
J. Vac. Sci. Technol. B **31**, 031205 (2013); 10.1116/1.4802917

Effect of polarity on Ni/InN interfacial reactions
Appl. Phys. Lett. **102**, 021607 (2013); 10.1063/1.4781768

Measurement of the Schottky barrier height between Ni-InGaAs alloy and In0.53Ga0.47As
Appl. Phys. Lett. **101**, 072103 (2012); 10.1063/1.4746254

Scanning transmission electron microscopy of ErAs nanoparticles embedded in epitaxial In 0.53 Ga 0.47 As layers
Appl. Phys. Lett. **86**, 111912 (2005); 10.1063/1.1885172

In situ controlled reactions and phase formation of thin films on GaAs
J. Vac. Sci. Technol. B **16**, 2280 (1998); 10.1116/1.590162

Reuse of AIP Publishing content is subject to the terms at: https://publishing.aip.org/authors/rights-and-permissions. Download to IP: 132.168.90.240 On: Wed, 05 Oct 2016 07:24:46

JOURNAL OF APPLIED PHYSICS **120**, 135304 (2016)

Reaction of Ni film with $In_{0.53}Ga_{0.47}As$: Phase formation and texture

Seifeddine Zhiou,[1] Tra Nguyen-Thanh,[2] Philippe Rodriguez,[1] Fabrice Nemouchi,[1] Laetitia Rapenne,[3] Nils Blanc,[2] Nathalie Boudet,[2] and Patrice Gergaud[1,a)]
[1]*Univ. Grenoble Alpes, F-38000 Grenoble, France and CEA, LETI, MINATEC Campus, F-38054 Grenoble, France*
[2]*Univ. Grenoble Alpes, F-38000 Grenoble, France and Inst. Néel, F-38054 Grenoble, France*
[3]*Univ. Grenoble Alpes, F-38000 Grenoble, France and CNRS, LMGP, F-38000 Grenoble, France*

(Received 12 July 2016; accepted 10 September 2016; published online 4 October 2016)

The solid-state reaction between Ni and $In_{0.53}Ga_{0.47}As$ on an InP substrate was studied by X-ray diffraction (XRD) and scanning transmission electron microscopy-energy-dispersive X-ray spectroscopy techniques. Due to the monocrystalline structural aspect of the so-formed intermetallic, it was necessary to measure by XRD a full 3D reciprocal space mapping in order to have a complete overlook over the crystalline structure and texture of the intermetallic. The formation of the intermetallic was studied upon several different Rapid Thermal Annealings on the as-deposited samples. Pole figures analysis shows that the intermetallic features a hexagonal structure ($P6_3/mmc$) with an NiAs-type (B8) structure. Although only one hexagonal structure is highlighted, the intermetallic exhibits two different domains characterized by different azimuthal orientations, axiotaxial relationship, and lattice parameters. The intermetallic phases seem to present a rather wide range of stoichiometry according to annealing temperature. The texture, structure, and stoichiometry of the intermetallic are discussed along with the evolution of lattice parameters of the Ni-InGaAs phase. *Published by AIP Publishing.* [http://dx.doi.org/10.1063/1.4963716]

I. INTRODUCTION

Among the hot topics driving the developments of new devices, the III–V materials (especially InGaAs alloys) represent serious candidates to replace silicon in elaborating sub 10 nm MOSFETs.[1] It was demonstrated that such components exhibit a significant increase of electron mobility throughout the channel and limit the band-to-band tunnel leakage.[2]

Thus, an ultra-low contact resistivity (below $10^{-9}\ \Omega\cdot cm^2$) is mandatory to reach entire device performances and will be therefore one of the key challenges for advanced node CMOS development. Historically, the developments of low-resistive contacts based on salicidation required a fine understanding of the silicide microstructure in order to control the solid-state reaction (SSR) of a metal film with the Si substrate. This point is crucial to control the process and its related contact resistivity. Therefore, there have been intense investigations on silicide technology (e.g., $TiSi_2$, $CoSi_2$, and NiSi)[3] over more than 25 years, leading to fundamental understanding on the peculiar microstructure observed for these compounds obtained by the SSR.[4,5] On the contrary, the knowledge turns out to be limited when it comes to ohmic metal contacts on III–V materials for MOSFET applications. For such alloys, salicide-like technology has been recently developed and it has been found that the Ni-$In_xGa_{1-x}As$ alloy is a promising material for the self-aligned metal source/drain (S/D) of $In_xGa_{1-x}As$ n-MOSFETs.[6,7] The solid-state reactions of Ni on GaAs have been initially described by Guivarc'h *et al.*[8] and Lahav *et al.*,[9] who demonstrated the formation of a multitude of intermetallics upon such reaction. The established ternary diagram showed successive steps of the interaction that lead to reacted layers consisting in one ternary phase or in a mixture of ternary and binary phases according to temperature. All the described phases have a hexagonal pseudocubic structure, in coherence with the well-known NiAs-type structure.[8] In the case of the Ni/InGaAs SSR, the structural properties, chemical composition, and texture of the so-formed intermetallic have been discussed recently in only few papers. For instance, Ivana *et al.* and Shekhter *et al.*[10–12] describe the hexagonal structure of the Ni-InGaAs with the 4:1:1:2 relative composition. Zhang *et al.*[13] found a similar composition ratio of 51:12:14:23. Shekhter *et al.*[11] also found the following orientation for the intermetallic Ni-InGaAs: $(10\bar{1}0)_{Ni\text{-}InGaAs}$ $||(001)_{InGaAs}$; $[0001]_{Ni\text{-}InGaAs}$ $||[01\bar{1}]_{InGaAs}$. However, a full understanding of the texture and phase formation is yet to be developed.

Thus, this paper aims to report the study carried out from the solid state reactions of Ni with InGaAs epitaxially grown on InP. We focus on phase formation and on the exhibited texture of these Ni-InGaAs intermetallic layers. We finally discuss the phase formation sequence, stoichiometry, and texture using axiotaxy considerations.

II. EXPERIMENTAL PART

A. Sample preparation

In this study, 200 nm thick $In_{0.53}Ga_{0.47}As$ layers were epitaxially grown by Metalorganic Chemical Vapour Deposition (MOCVD) on 100 mm, (100) oriented InP wafers. We will refer indifferently to this III–V compound by InGaAs or $In_{0.53}Ga_{0.47}As$ in this paper. Afterwards, a 20 nm layer of Ni was deposited on the $In_{0.53}Ga_{0.47}As$ by means of Radio Frequency Physical Vapor Deposition

a)Electronic mail: patrice.gergaud@cea.fr

Reuse of AIP Publishing content is subject to the terms at: https://publishing.aip.org/authors/rights-and-permissions. Download to IP: 132.168.90.240 On: Wed, 05 Oct 2016 07:24:46

(RF-PVD). The metallic layer is capped with a TiN thin film to prevent atmosphere contamination. Before the Ni/TiN metal deposition, argon direct plasma *in situ* pretreatments to remove native oxides were carried out using a RF1 power of 130 W and a RF2 power of 310 W. The *in situ* etching process was calibrated on thermal silicon oxide to obtain the process time versus silicon oxide equivalent thickness of 2.5 nm. *In situ* pretreatment and metal deposition were carried out in a 300 mm Applied Materials Endura platform usually dedicated to the silicide process. Full description of the samples is given in Figure 1. The samples were annealed at different temperatures during 60 s and under N_2 flow using Rapid Thermal Annealing (typically 250 °C, 300 °C, 350 °C, 450 °C, and 550 °C).

B. Experimental setup

In the following paragraph, we describe the experimental setup that was put in place in order to keep track of all possible diffraction signals from the intermetallic, since no powder diffraction file is available yet for the studied phase. By this way, we make sure that we identify the right space group for the assumed monocrystalline intermetallic phase. This point is of a great importance to characterize the intermetallic properly. For example, early studies of Ni on Si reaction wrongly identified an intermediate phase as orthorhombic Ni_3Si_2,[14] while a complete texture study over large parts of the reciprocal space undertook by Gaudet *et al.*[15] showed that this phase is rather a hexagonal one. To this end, X-ray diffraction 3D-Reciprocal Space Mapping (3D-RSM) experiments were performed on the BM02 beamline, the French Collaborating Research Group (CRG) beamline, at the European Synchrotron Radiation Facility (ESRF). They were carried out at an energy of 9 keV in order to prevent Ga and As fluorescence. We used a 6-circle goniometer but we will refer in this paper to the χ, ϕ, and 2θ angles as the angles of a conventional 4-circle diffractometer.

A large hybrid pixel detector manufactured by imXPAD[16,17] using Si diodes and situated at 20 cm from the sample was employed to collect the diffracted beams. Such a detector allows collecting data over a relatively wide range of the reciprocal space at one time. The setup of the diffractometer and detector was such that we were capable of measuring, at a given tilt angle of the sample (ϕ), a range of 30° of 2θ during a one-shot-measurement. Two values of the χ tilt were chosen to cover a range going from 0° to about 70° depending on the 2θ position, and multiple measurement steps were added by rotating the sample around its normal to the surface (ϕ) to obtain full pole figures over 360°. The step of the ϕ measurement is $\Delta\phi = 5°$, which is sufficient if the mosaicity of the crystallites is not too important but can result in discrepancies of intensities between poles if the mosaicity is important. As the 2D detector has some dead rows and columns, we did each acquisition at $\nu = 0°$ and 2° (in-plane rotation of the detector) to measure all possible diffraction information. These same steps were also carried on the LaB_6 powder sample in order to perform the proper calibrations. In this configuration, several Debye-Scherrer rings were recorded on the same image with a 10 s exposure time. Thus, the acquisition time is considerably reduced compared to standard θ–2θ measurements using the point detector. Data reduction was performed with our homemade DEVA software,[18] stereographic projections and pole figure simulations were carried out on CaRIne Crystallography 3.1,[19] and drawings of crystal structures were done using VESTA 3.1.8.[20]

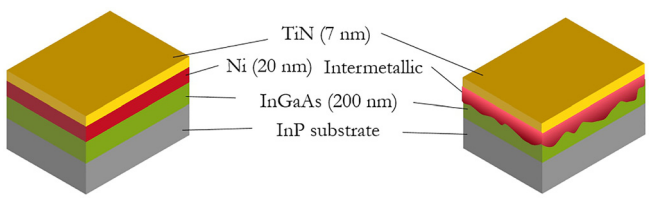

FIG. 1. Scheme of the stacks in the sample as-deposited (left) and after solid-state reaction (right).

C. Miscut measurement

In order to enhance the $In_{0.53}Ga_{0.47}As$ layer quality, the surface of the $In_{0.53}Ga_{0.47}As$/InP wafer is miscut when prepared. We use the method described by Covita *et al.*[21] to measure the miscut angle and determine its direction.

The measurements were performed on a Rigaku Smartlab diffractometer using the in-plane configuration. First, we pre-aligned the sample surface playing with the two rotations above the azimuthal rotation axis in order to put in coincidence the azimuthal axis and the normal to the surface. Then, we performed rocking curve measurements around the (200) plane for several azimuthal positions (360° with a step of 5°). The difference $\Delta(\Omega)$ between the measured peak position Ω and the peak reference position Ω_0 according to the azimuthal position is then plotted (Figure 2). A sinusoidal-like curve is obtained and the miscut angle corresponds to the amplitude of this curve. Using the same sample alignment on the sample holder, the pole figure of the {220} planes of the substrate was then measured, and the direction of the miscut was fixed. This approach was validated on an industrial-quality silicon wafer, where the measured miscut at the surface is 0.03° which is insignificant and can be considered as the instrumental error as the manufacturer given value of the miscut for the Si substrate is also close to 0°. As for the InP substrate, we obtain miscut angles of about 0.22°.

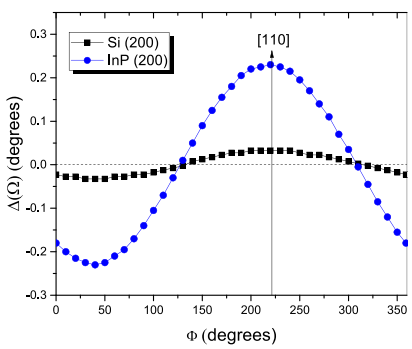

FIG. 2. $\Delta(\Omega)$ evolution of the (2 0 0) peak position of the (2 0 0) planes for Si (squared black) and InP (dotted blue) according to Φ.

Reuse of AIP Publishing content is subject to the terms at: https://publishing.aip.org/authors/rights-and-permissions. Download to IP: 132.168.90.240 On: Wed, 05 Oct 2016 07:24:46

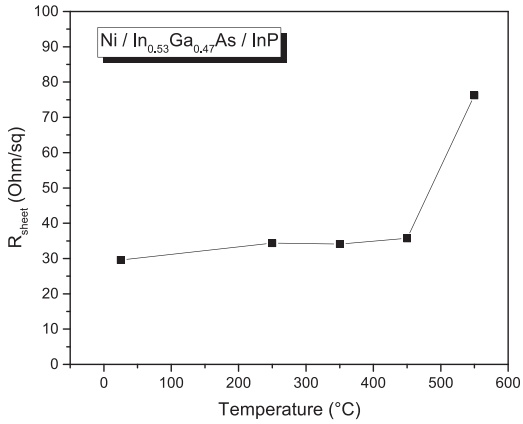

FIG. 3. Evolution of the sheet resistance of the TiN/Ni-InGaAs layers according to annealing temperature.

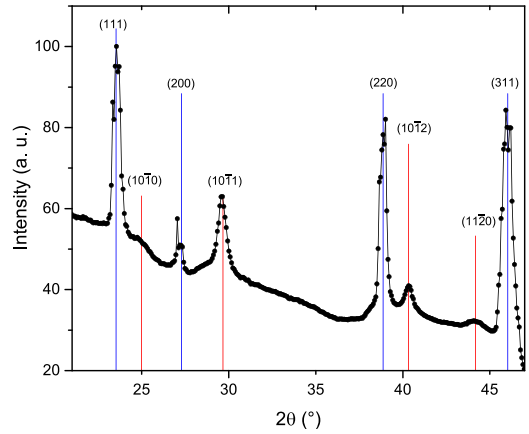

FIG. 4. X-Ray diffractogram of a sample after a 350 °C annealing. Red lines correspond to the intermetallic peak positions and blue lines correspond to the InP/$In_{0.53}Ga_{0.47}As$ peak position. X-Ray energy was set to 9 keV.

III. RESULTS

A. Electrical results

Figure 3 exhibits the sheet resistance of the TiN/Ni layers on the InGaAs/InP material according to rapid thermal annealing temperature. Sheet resistance of the 7 nm layer of TiN is 433.9 Ω/sq, and several measurements were carried out on each sample. The standard deviation of the values is about 0.1–0.2 Ω/sq. Thus, even with small variations, the evolution of sheet resistance values is significant. As deposited (as-dep), we measure the sheet resistance of the TiN and Ni metallic layers. From 250 to 350 °C, the sheet resistance increases. This phenomenon corresponds to the initiation of the Ni-InGaAs intermetallic formation. As intermetallic phases have higher resistivity than metallic layers, the global sheet resistance is slightly increasing. At 250 °C, the sheet resistance gently decreases. At this point, we may assume that we have formed the less resistive Ni-InGaAs intermetallic. From 350 to 450 °C, the sheet resistance increases again. We can link this evolution with the degradation of intermetallic properties with the increasing thermal budget. As the sheet resistance value considerably increases at 550 °C, we can postulate that the intermetallic composition/nature has probably changed. The microstructure analysis described in Sec. III B is necessary to go further into interpretation.

B. Structure of the intermetallic

X-Ray diffraction was used to study the structure of the intermetallic. Two kinds of information have been extracted from the multiple 2D datasets we measured by XRD: (i) De-textured 2θ diffractograms (see Figure 4) were obtained by summing over χ and ϕ the Debye rings of all the 2D snapshots; (ii) pole figures (see for instance Figures 5(a) and 5(b) and Appendix A were reconstructed for several hkl reflections (or 2θ angles)). From the indexation of these diffractograms and from the symmetry of the pole figures, and in agreement with the results published by Shekhter *et al.*,[11] we identified clearly the intermetallic phases that appear during SSR have a hexagonal structure and determined the space group as the $P6_3/mmc$ with hexagonal pseudocubic-like lattice parameters that varies according to either orientation or annealing temperature. The unit cell of the hexagonal structure contains two formulas units[8] (see Figure 6); the metal atoms occupy the *2a* at (0,0,0) and (0,0, $\frac{1}{2}$) sites and the non-metal atoms occupy the

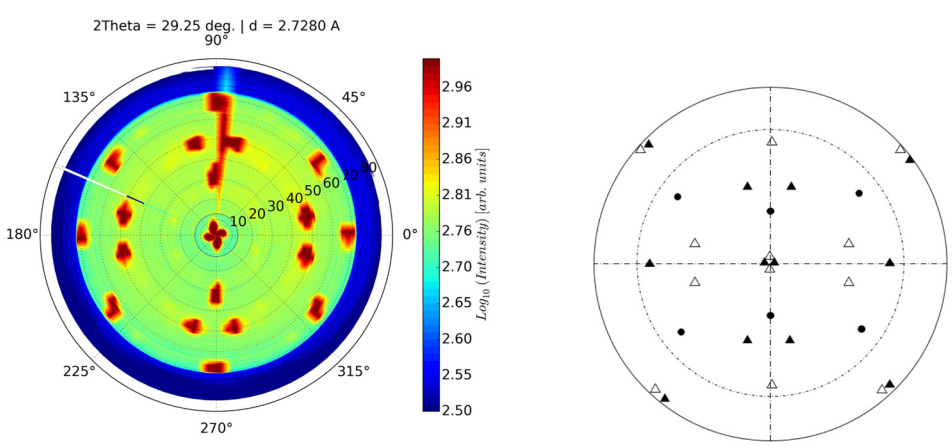

(a) (b)

FIG. 5. (a) X-ray diffraction pole figures of the Ni/InGaAs/InP sample (after a 450 °C RTA annealing). The fixed 2θ angle was 29.25° corresponding to the intermetallic $\{10\bar{1}1\}$ reflections. The concentric dashed circles correspond to the χ angle landmarks with a 10° step. The intensity line at $\phi = 90°$ is due to an experimental artifact, (b) Stereographic projection of the $(10\bar{1}1)$ planes of the intermetallic hexagonal structure for the different orientations given in Table I. Only the poles included in the dashed circle were measured.

Reuse of AIP Publishing content is subject to the terms at: https://publishing.aip.org/authors/rights-and-permissions. Download to IP: 132.168.90.240 On: Wed, 05 Oct 2016 07:24:46

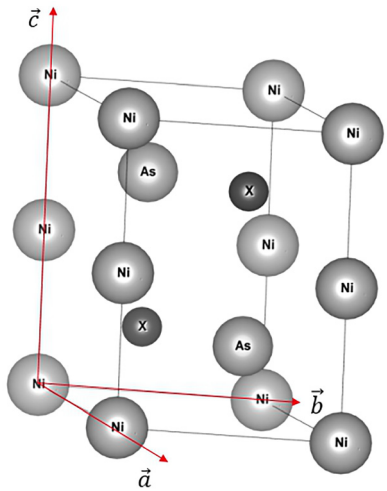

FIG. 6. Reduced lattice of the NiAs hexagonal structure. The atom position marked by X corresponds to *(2d)* sites.[8]

2c sites at the $(\frac{1}{3}, \frac{2}{3}, \frac{1}{4})$ and $(\frac{2}{3}, \frac{1}{3}, \frac{3}{4})$ positions. Moreover there are two additional sites *2d* at $(\frac{1}{3}, \frac{2}{3}, \frac{1}{3})$ and $(\frac{2}{3}, \frac{1}{3}, \frac{1}{4})$ positions for the metal which can be partially, fully, or non-occupied. In this case, Ni atoms occupy the *2a* and potentially *2d* sites, while In, Ga, and As occupy the *2c* sites.

This hexagonal phase is the only one we observe whatever the RTA temperature. From the de-textured diagram, we extracted the a and c lattice parameters of the structure according to annealing temperature (see Figure 7).

C. Texture of the intermetallic

Our results exhibit some discrepancies with the works cited previously, especially concerning the texture of the intermetallic. No reaction occurs up to 250 °C annealing temperature as the X-ray diffraction results show no new peak or new pole after an annealing at such temperature. At 300 °C, the intermetallic phase shows up and Ni is fully consumed. This phase is still observed at 450 °C and at 550 °C with the same texture and orientation. Actually, we observe multiple poles for the pole figure at $2\theta = 29.25°$ (Figure 5(a)). Poles at $\chi = 33°$ and $\chi = 65°$ correspond to the projection of $(10\bar{1}1)$ plane of the intermetallic phase on the $(10\bar{1}0)$

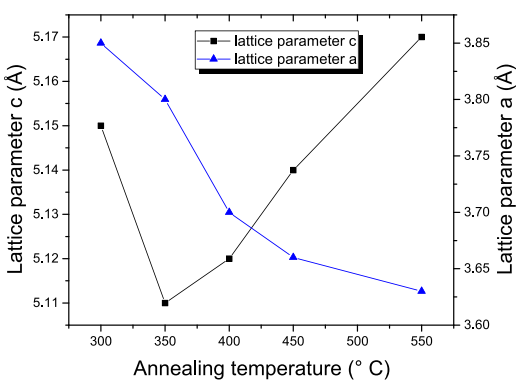

FIG. 7. Evolution of the hexagonal lattice parameters a and c of the intermetallic according to the annealing temperature.

TABLE I. Summary of the orientations observed for the so-formed intermetallic for Ni/InGaAs/InP initial stacks. Each symbol corresponds to an orientation in Figure 5(b).

Symbol	Number	Orientation
●	1	$(10\bar{1}0)_{\text{Ni-InGaAs}} \,\|\|\, (001)_{\text{InGaAs}};\ [0001]_{\text{Ni-InGaAs}} \,\|\|\, [01\bar{1}]_{\text{InGaAs}}$
▲	2	$(10\bar{1}1)_{\text{Ni-InGaAs}} \,\|\|\, (001)_{\text{InGaAs}};\ [1\bar{2}10]_{\text{Ni-InGaAs}} \,\|\|\, [0\bar{1}\bar{1}]_{\text{InGaAs}}$
△	3	$(10\bar{1}1)_{\text{Ni-InGaAs}} \,\|\|\, (001)_{\text{InGaAs}};\ [1\bar{2}10]_{\text{Ni-InGaAs}} \,\|\|\, [01\bar{1}]_{\text{InGaAs}}$
	4	$(10\bar{1}0)_{\text{Ni-InGaAs}} \,\|\|\, (001)_{\text{InGaAs}};\ [0001]_{\text{Ni-InGaAs}} \,\|\|\, [0\bar{1}\bar{1}]_{\text{InGaAs}}$

plane along the [0 1 1] direction of the substrate (see orientation 1 in Table I) and the poles at $\chi = 4°$, $\chi = 49°$, and $\chi = 67°$ correspond to the projection of $(10\bar{1}1)$ on the $(10\bar{1}1)$ plane along two in-plane directions of the hexagonal structure (orientations 2 and 3).

In summary, for the Ni/InGaAs/InP substrates, the intermetallic exhibits the orientations 1, 2, and 3 described in Table I. For simplification purposes, we denote the orientation where the $(10\bar{1}0)$ planes of the intermetallic are parallel to the substrate surface as group A orientation. The orientations where the $(10\bar{1}1)$ planes of the intermetallic are parallel to the substrate surface are denoted as group B. All the observed orientations of the hexagonal structure are given in Table I and a complete stereographic projection with the corresponding orientation for each pole is given in Figure 5(b).

Due to the fact that all variants are oriented along the $\langle 110 \rangle$ vector group of the substrate, each domain group should exhibit two in plane variants tilted by 90° the one against the other. However, only one azimuthal variant was identified for group A domains. The missing azimuthal orientation for group A domains is denoted as orientation 4 in Table I.

We also report the formation of a superstructure based on the parent hexagonal lattice and resulting probably from an order on the distribution of Ni atoms on the *2d* sites.[8,22] Several lattice planes related to diffraction from a superstructure were identified. By indexing the planes and verifying stereographic projections, superstructures were put in evidence for both groups. The first one yields the same orientation of group B (for both azimuthal variants) and has $(2a \times 3c)$ lattice parameters. The second one yields the same orientation of group A and also has $(2a \times 3c)$ lattice parameters. Examples of diffraction from the superstructure are given in Figures 8(a) and 8(b), which describe, respectively, the pole figures of the $\{3\bar{1}\bar{2}1\}$ and the $\{10\bar{1}7\}$ planes of the superstructures. Apart from a change in the intensity of peaks, indicating either a change in the quality of ordering or can be related to the proportion of the corresponding elementary lattice, no other superstructure was resolved or further evolution was measured according to annealing temperature. The corresponding stereographic projections are shown, respectively, in Figures 8(b) and 8(d). For the sake of clarity, the stereographic projections in Figure 8(b) yield just one azimuthal variant. The other azimuthal variant can be obtained by simply rotating the stereographic projection by 90°. The second azimuthal variant for group B can be seen on its corresponding pole figure in Figure 8(a). However,

Reuse of AIP Publishing content is subject to the terms at: https://publishing.aip.org/authors/rights-and-permissions. Download to IP: 132.168.90.240 On: Wed, 05 Oct 2016 07:24:46

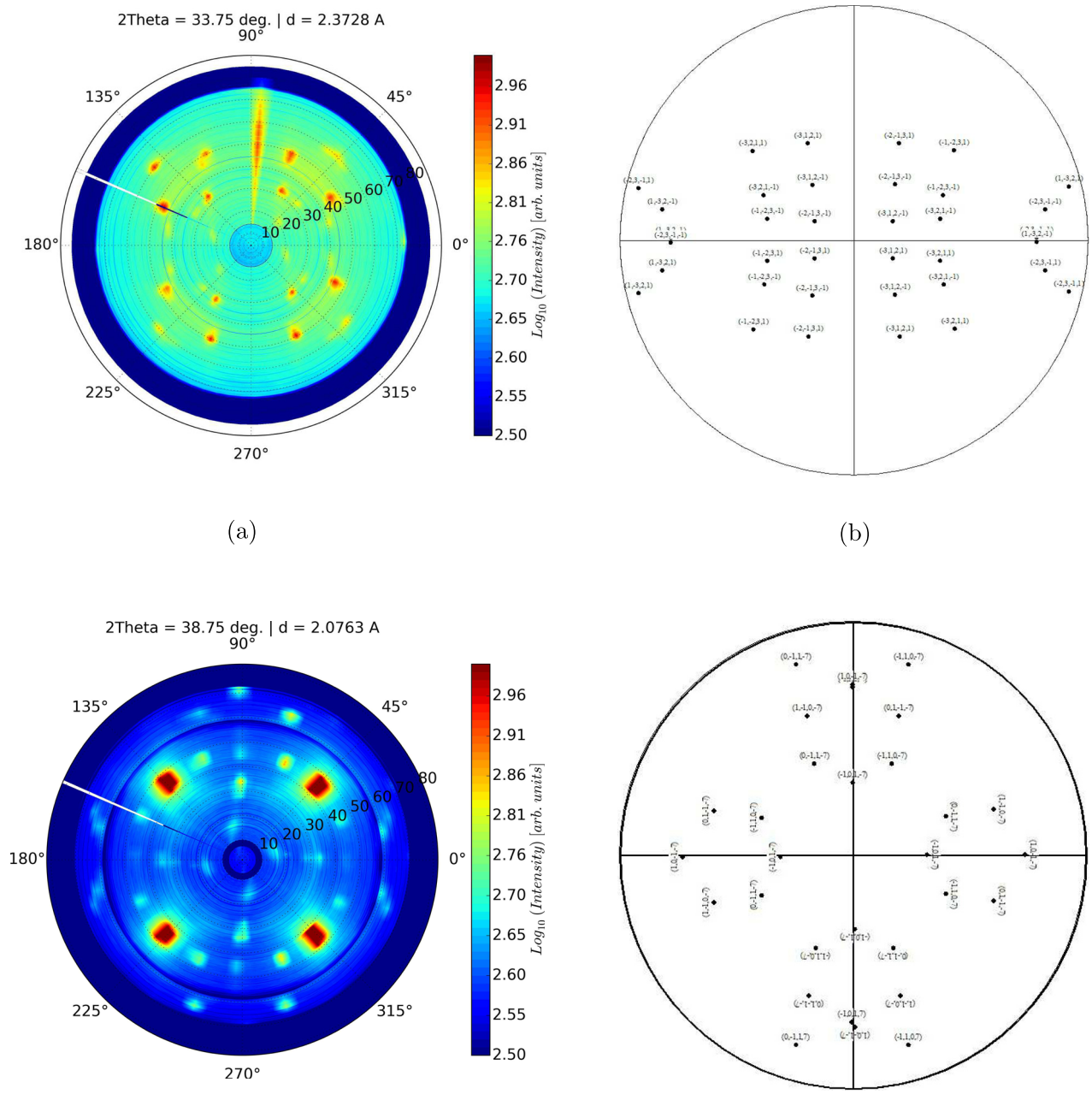

FIG. 8. Pole figures of respectively: (a) $\{3\bar{1}\bar{2}1\}$ planes and (c) $\{10\bar{1}7\}$ planes, and respectively their corresponding stereographic projections: (b) for $\{3\bar{1}\bar{2}1\}$ planes and (d) for $\{10\bar{1}7\}$ planes. Extra poles on (c) correspond to nearby diffraction peaks from the substrate and main intermetallic.

several poles of the second variant are superposed to the first one and thus can be hardly distinguished on the pole figure.

D. Domain quantification

From Figure 15 in Appendix B, we can clearly see that intensities from poles that correspond to group A and group B domains are not equal according to annealing temperature. We quantified group A and group B domains according to annealing temperature by measuring the integrated intensities from two $(10\bar{1}1)$ poles each corresponding to a domain group. Figure 9 shows the ratio of the integrated intensities from these two poles, along the χ, ϕ, and 2θ angles. It shows that from 300 °C to 450 °C group A domains are predominant and at 550 °C group B domains are predominant. Due to the relatively important step $\Delta\phi = 5°$ used to acquire the pole figures, and due to a lower mosaicity of the intermetallics formed at 550 °C, poles at 48° in Figure 15(d) appear to have different intensities. However, homogeneity of the intensities was further verified through a measurement with a finer step $\Delta\phi = 1°$.

E. STEM-EDS measurements

STEM-EDS maps were carried out on a TEM JEOL 2100F. Sample preparation consisted of preparing a substrate/film/glue/film/substrate "sandwich" and polishing was performed by a tripod bevel to 10 μm followed by Ar ion milling until perforation of the interface.

Reuse of AIP Publishing content is subject to the terms at: https://publishing.aip.org/authors/rights-and-permissions. Download to IP: 132.168.90.240 On: Wed, 05 Oct 2016 07:24:46

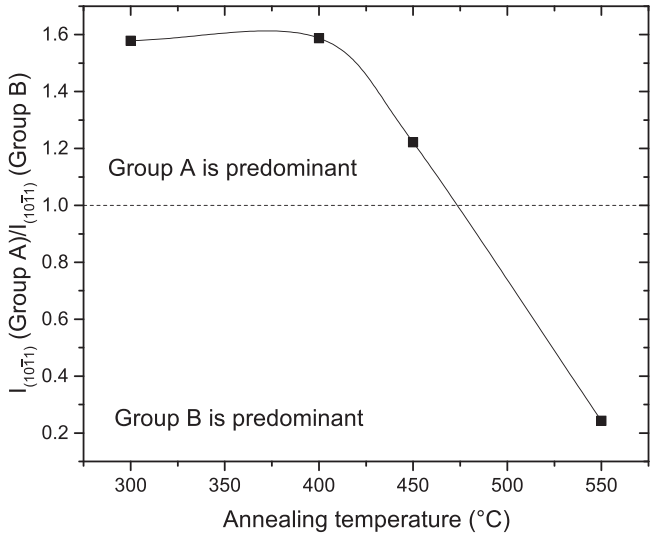

FIG. 9. Ratio of the relative intensities between $I_{(10\bar{1}1)}$ of group A and $I_{(10\bar{1}1)}$ of group B according to temperature.

Samples annealed at 300 °C and 550 °C were measured (see Figure 10). The STEM-EDS maps show that at low annealing temperatures, In, Ga, and As are nearly at their nominal stoichiometry inside the intermetallic compound. On the contrary, at higher annealing temperatures, starting at 450 °C, the proportion of these elements inside the intermetallic lattice is no longer the same as their nominal composition (not shown here). This observation suggests an out-diffusion of Ga and In during the thermal annealing and the formation of NiAs at higher temperature. Moreover, at the highest annealing temperature, the film is highly agglomerated suggesting important structural changes. A similar degradation process of germano-silicides was discussed by Jarmar *et al.*[23] The agglomeration may be related to the strong increase of the resistivity at 550 °C in Figure 3.

IV. DISCUSSION

A. Texture of the intermetallic

A more detailed observation of the $(10\bar{1}1)$ pole figure shows that there is a shift of poles from the center of about 3°. In fact, if the $(10\bar{1}1)$ planes were perfectly parallel to the sample surface ((001) of InGaAs), the 4 diffraction poles would be merged into a single pole located at (ϕ,χ) (0°,0°). The presence of a shift indicates that the $(10\bar{1}1)$ planes are slightly tilted from the sample surface. This kind of behavior was observed for Ni_2GaAs and $NiAs_{1-x}Al_x$ hexagonal compounds.[9,24] Actually, face-centered cubic lattices like the blende structure (GaAs, AlAs, and InGaAs) can be described in a hexagonal lattice with $c/a = \sqrt{3}/\sqrt{2}$, with the $(10\bar{1}1)_h$ and $(0001)_h$ planes rigorously parallel, respectively, to the $(001)_c$ and $(111)_c$ of the cubic lattice (Figure 11(a)). Thus, we obtain the following crystallographic relationships: $(10\bar{1}1)_h \,||(001)_c$ and $(0001)_h \,||(111)_c$. In this ideal case, on the $(001)_c$ oriented substrate, the $(10\bar{1}1)_h$ plane is perfectly the $(001)_c$ plane. Further, for any hexagonal lattice hexagonal lattice presenting a c/a ratio slightly different from $\sqrt{3}/\sqrt{2}$ (the structure is then called pseudocubic hexagonal lattice), the precedent rule is no longer rigorously respected. In theory, the hexagonal pseudocubic compounds will tend to be oriented in a way to satisfy the $(0001)_h \,||(111)_c$ condition. Thus, no longer rigorously parallel to the $(001)_c$ and these rigorously parallel to the $(001)_c$ and these two planes will form an angle α which can be measured through X-ray diffraction. This angle is as large as the c/a ratio is far from $\sqrt{3}/\sqrt{2}$.

Assuming that $(0001)_h \,||(111)_c$, we can define the angle between $(0001)_h$ and $(10\bar{1}1)_h$ as β. The tilt angle α can be defined as the difference between the angle $\beta_{c/a=\sqrt{3}/\sqrt{2}}$ in the case of an ideal hexagonal pseudocubic and $\beta_{c/a\neq\sqrt{3}/\sqrt{2}}$ in the case of a regular hexagonal pseudo cubic

$$\alpha = \beta_{c/a=\sqrt{3}/\sqrt{2}} - \beta_{c/a\neq\sqrt{3}/\sqrt{2}}. \quad (1)$$

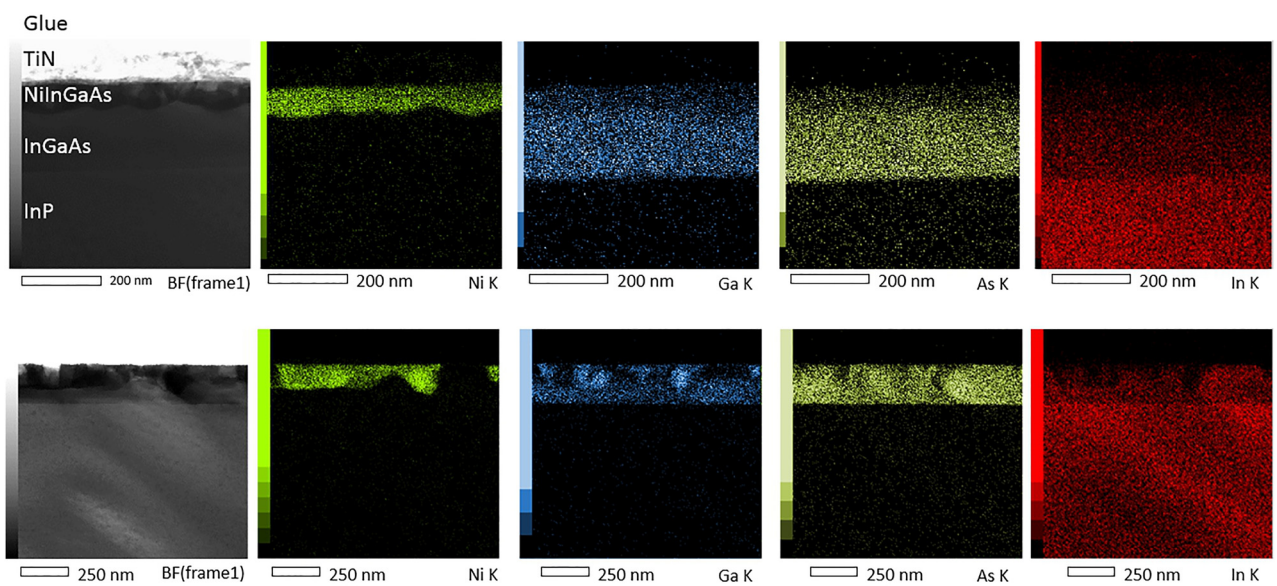

FIG. 10. Bright Field (BF) TEM images and element map using STEM EDS of the samples annealed at 300 °C (Top) and 550 °C (Bottom).

Reuse of AIP Publishing content is subject to the terms at: https://publishing.aip.org/authors/rights-and-permissions. Download to IP: 132.168.90.240 On: Wed, 05 Oct 2016 07:24:46

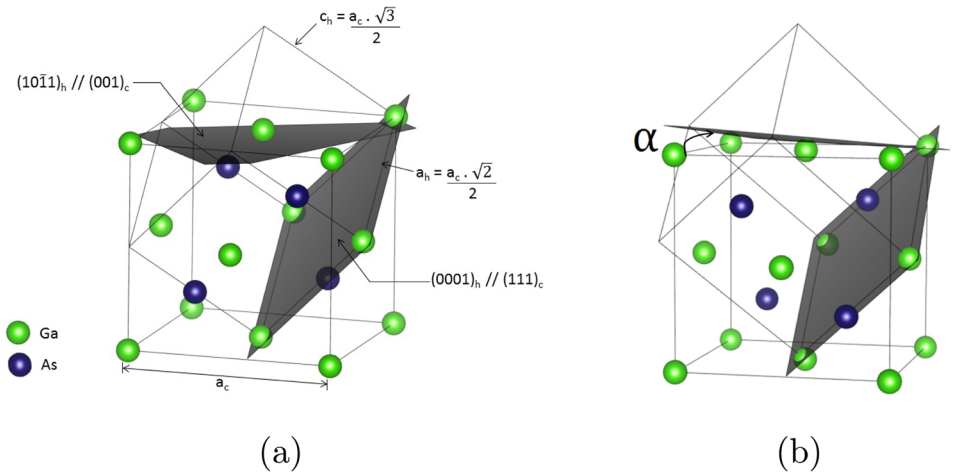

FIG. 11. (a) Transformation scheme of the cubic unit cell of the zinc blende-type structure in a hexagonal lattice with an ideal ratio of $c/a = \sqrt{3}/\sqrt{2}$ (adapted from Lahav[9]), (b) Transformation scheme of cubic unit cell of the zinc blende-type structure in a hexagonal lattice with a ratio of 1.4, the angle between the $(001)_c$ and $(10\bar{1}1)_h$ is denoted α.

The angle between two planes $(h_1k_1l_1)$ and $(h_2k_2l_2)$ in the hexagonal structure can be calculated as the following:[25]

$$\cos(\Phi) = \frac{h_1h_2 + k_1k_2 + \frac{1}{2}(h_1k_2 + k_1h_2) + \frac{3a^2}{4c^2}(l_1l_2)}{\sqrt{\left\{\left[h_1^2 + k_1^2 + h_1k_1 + \frac{3a^2}{4c^2}(l_1^2)\right]\left[h_2^2 + k_2^2 + h_2k_2 + \frac{3a^2}{4c^2}(l_2^2)\right]\right\}}}. \quad (2)$$

Using Equation (2) to calculate the β angle between the (0001) and the $(10\bar{1}1)$ planes, we obtain

$$\cos(\beta) = \frac{\sqrt{\frac{3a^2}{4c^2}}}{\sqrt{1 + \frac{3a^2}{4c^2}}}. \quad (3)$$

Using Equation (3) into (1), the tilt angle α can be calculated using the lattice parameters of the hexagonal structure in the following manner:

$$\alpha = \cos^{-1}\left(\frac{1}{\sqrt{3}}\right) - \cos^{-1}\left(\frac{\sqrt{\frac{3a^2}{4c^2}}}{\sqrt{1 + \frac{3a^2}{4c^2}}}\right). \quad (4)$$

Figure 12 shows the evolution of the α angle as measured and as calculated according to annealing temperature. The evolution of the c/a ratio is also plotted in the same figure. At 300 °C, $\alpha_{measured}$ and $\alpha_{calculated}$ exhibit a notable difference. At 350 and 450 °C, the axial ratio c/a increases which might be related to stoichiometry changes, and along, the value of $\alpha_{measured}$ and $\alpha_{calculated.}$ Finally, at 550 °C, the axial ratio c/a strongly increases and likewise $\alpha_{calculated}$ and $\alpha_{measured.}$ While the evolution trend is the same for both $\alpha_{calculated}$ and $\alpha_{measured}$, we state that there is a shift between these two values that increases according to annealing temperature. This can be explained by the fact that the lattice parameter calculation was performed at room temperature after the annealing. An anisotropic thermal expansion during the sample cooling will subsequently change the c/a ratio from its value at the formation of the intermetallic. Considering that no further rotation of the $(10\bar{1}1)$ planes would occur after the anisotropic expansion of lattice parameters, the measured and calculated values of α would be then different. No tilt was measured for group A orientation as the measured pole positions corresponding to this orientation matches the calculated ones. The additional orientations were not observed by Shekhter *et al.*[11] This is likely due to the low annealing temperature used to form the Ni-InGaAs alloy (i.e., 250 °C), and the probable late formation of group B domains.

B. Miscut influence on azimuthal orientations

Shekhter *et al.*[11] observed the same missing azimuthal variant for group A intermetallics and stated that the presence of atomic steps at the surface of the substrate can

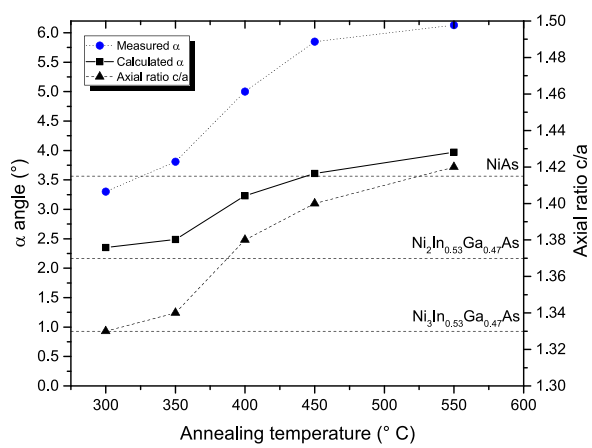

FIG. 12. Measured and calculated tilt angles α and c/a ratio according to the annealing temperature for Ni/InGaAs/InP samples.

Reuse of AIP Publishing content is subject to the terms at: https://publishing.aip.org/authors/rights-and-permissions. Download to IP: 132.168.90.240 On: Wed, 05 Oct 2016 07:24:46

induce such anisotropy. Indeed, when the substrate presents a low angle miscut that prevents (100) planes from being completely parallel to the sample surface, it can loose its four-fold symmetry along with the deposited InGaAs layer. This symmetry reduction may lead to the formation of the intermetallic along some preferred directions that can be explained by the epitaxial or axiotaxial relationship.[5]

We identified the miscut direction as the one oriented along [110] on different samples. Such a configuration introduces an asymmetry between ⟨110⟩ directions that lie at the surface of the sample. Nevertheless, we could not relate the direction of the miscut on each sample with the ⟨110⟩ direction along which the hexagonal intermetallic is aligned. Thus, we conclude that such anisotropy is likely not due to the presence of a miscut at the surface of the sample.

C. Stoichiometry

Figure 12 shows the evolution of the axial ratio c/a of the hexagonal intermetallic according to the annealing temperature with two major limits: NiAs and $Ni_3In_{0.53}Ga_{0.47}As$. At 300 °C, the c/a corresponds to the lattice parameters of Ni_3GaAs and likely so corresponds to $Ni_3In_{0.53}Ga_{0.47}As$ since In and Ga exhibit close covalent radii (respectively, 0.142 nm and 0.122 nm). The c/a ratio increases significantly at 400 °C and is comparable to the one of $Ni_2In_{0.53}Ga_{0.47}As$. At 550 °C, the axial ratio is very close to the axial ratio of NiAs. This is in agreement with the STEM-EDS results (see Figure 10). Moreover, oriented facets belonging to group B at 54° appear clearly after a 550 °C annealing (in Figure 10, and related to poles at 54° at Figure 5(a)), and thus correspond to a growth along the [111] axis of the substrate. Moreover, group B domains are more predominant at higher temperature (see Figure 9). A faster diffusion along the growth axis of group B domains at higher temperature can explain this phenomenon (*c* axis).

Group A domain orientation is the same as mentioned for a similar SSR by Shekhter *et al.*[11] This orientation can be resolved by considering an axiotaxial alignment between the $(10\bar{1}0)$ planes of group A domains and the (110) planes of the substrate. Taking into account this axiotaxy, every set of four (110) planes of the substrate should meet every set of five $(10\bar{1}0)$ planes of the hexagonal phase. No axiotaxial lines were measured on pole figures but rather fixed in the plane direction along [110]. We also consider an axiotaxial alignment to calculate the lattice mismatch according to the interplanar distance of the (0001) planes of the intermetallic and the one of the (111) plane of the substrate. Indeed, every set of three (0001) hexagonal planes should meet every set of two (111) substrate planes at 2 points.[26] The occurrence of an axiotaxy, where lattice planes of the intermetallic are aligned with lattice planes of the substrate, is a possible explanation for the group B orientation. Moreover, the high roughness of the so-formed film is likely to favor the occurrence of an axiotaxy-like alignment.[5] While no tilted fiber texture (typical of axiotaxy) was observed on pole figures, we can consider the following: the [111] axis is a three-fold rotational axis that can easily adjust with the six-fold rotational c axis of the hexagonal structure. Thus, the growth occurs only through epitaxial relationship with the substrate as it was described for ϵ-NiGe by De Schutter *et al.*[26] (see Table II). The calculated mismatch according to the description of the alignments at the beginning of this paragraph is summarized in Table III for both intermetallic domains.

The formation of the intermetallic in the Ni/InGaAs system is obviously a way to minimize the Gibbs free energy when a certain amount of thermal budget brought to by the rapid thermal annealing. In this case, and contrary to the formation of silicides, only one crystalline structure is formed, and the prime intermetallic formed tends to only change its stoichiometry in order to keep minimization of the Gibbs free energy. Actually, the surface energy terms can also particularly be lowered by stoichiometry adjustment. Ni has been proven to be the diffusing species during the Ni-InGaAs solid-state reaction.[27] The nickel diffusion is the dominant controlling mechanism for the intermetallic formation at lower thermal budgets (lower RTA annealings). Once all the metal has been entirely consumed and thermal budget is high enough, the intermetallic tends to expel metal atoms from the *2d* positions and also Ga and In atoms in order to reach the NiAs phase. This fairly explains the evolution from a $Ni_3In_{0.53}Ga_{0.47}As$ structure to a $Ni_2In_{0.53}Ga_{0.47}As$ structure and finally NiAs-like stoichiometry.

This result is in agreement with the ternary phase diagram established by Guérin *et al.*[28] for Ni, Ga, and As alloys. The phase diagram states that the different Ni-GaAs intermetallics belong all to the $P6_3/mmc$ space group. Five phases were identified with different homogeneity ranges and different ordered/disordered structures (i.e., presenting a superstructure or not). The only stable phase for the Ni, Ga, and As system is the NiAs phase. In our case, we had expect to form the richest phase in Ni (where $n(Ni) > 3$) first according to the Cu_3Au rule.[29] Nevertheless, this phase is disordered according to Guérin, and we observe only ordered structures throughout the different annealing. Thus, it is likely that we start by forming $Ni_3In_{0.53}Ga_{0.47}$ and ending up with NiAs and NiAs-based solid solutions. This comparison with the ternary phase diagram is reasonable since In is completely miscible in the GaAs lattice where it occupies Ga sites.

To conclude, if one defines a crystalline phase as a homogeneous crystal structure accepting a certain range of stoichiometry, the Ni/InGaAs system presents therefore a sequence of 3 phases with the same B8 crystallographic structure but with different stoichiometry: $Ni_3In_{0.53}Ga_{0.47}As$, $Ni_2In_{0.53}Ga_{0.47}As$, and NiAs. The shift from a stoichiometry to another is probably not continuous but during the transition, the average measured c/a ratio represents a fraction mixed of at least two c/a ratios corresponding to at least two distinct phases. Indeed, we can consider that the intermetallic

TABLE II. Rewritten orientations of group B domains according to a growth along the [111] axis of the $In_{0.53}Ga_{0.47}As$.

Number	Orientation
2	$(0001)_{Ni\text{-}InGaAs} \parallel (111)_{InGaAs}$; $[1\bar{2}10]_{Ni\text{-}InGaAs} \parallel [0\bar{1}\bar{1}]_{InGaAs}$
3	$(0001)_{Ni\text{-}InGaAs} \parallel (111)_{InGaAs}$; $[1\bar{2}10]_{Ni\text{-}InGaAs} \parallel [01\bar{1}]_{InGaAs}$

Reuse of AIP Publishing content is subject to the terms at: https://publishing.aip.org/authors/rights-and-permissions. Download to IP: 132.168.90.240 On: Wed, 05 Oct 2016 07:24:46

TABLE III. Mismatch of $(10\bar{1}0)$ planes of group A according to (110) planes of the substrate and those of (0001) planes of group B according to (111) planes of the substrate.

Orientation	300 °C	350 °C	400 °C	450 °C	550 °C
Group A	0.5%	−0.7%	−3.5%	−4.6%	−5.5%
Group B	−1.3%	−0.5%	−0.7%	−1.1%	−1.7%

compound phase transition is effectively sharp but appears rather as a smooth one (see Figure 12).

V. CONCLUSION

We studied the phase formation when a reaction occurs between Ni thin films with $In_{0.53}Ga_{0.47}As$ on InP substrates. 3D-RSM developed on the ESRF synchrotron was used in order to identify the so-formed intermetallic. De-texturing results indicate that there is a formation of a single NiAs-type (B8) hexagonal structure. There is however a phase transition according to the annealing temperature which is not a sharp one but appears as a smooth transition from a Ni-rich phase to NiAs. This result was further confirmed using STEM-EDS results and is coherent with the early results on Ni/GaAs metallization. Pole figure reconstruction indicates that there is a formation of two domain groups and axiotaxial alignments along with symmetrical considerations that were necessary to explain the intermetallic/substrate relationship.

Indeed, we demonstrate that group A domains have their $(10\bar{1}0)$ m-plane parallel to the sample surface. Moreover, this domain group exhibits orientation reduction which could not be attributed to the presence of miscut at the surface of the sample. Group B domains, however, grow along the [111] direction of the semiconductor and are more predominant at higher annealing temperatures (starting from 550 °C). Furthermore, group B domains have their $(10\bar{1}1)$ plane nearly parallel to the sample surface. This tilt from the surface is directly related to the lattice parameter of the intermetallic and also the relationship between the zinc-blende structure and B8 hexagonal structure. Finally, we emphasize on the fact that within the proposed phases presented in this study, only the NiAs one is stable. Hence, any formed phase other than NiAs for the (Ni, In, Ga, and As) system is not a stable one but rather a metastable phase.

ACKNOWLEDGMENTS

This work was supported by the LabEx Minos ANR-10-LABX-55-01 and funded by the French National Research

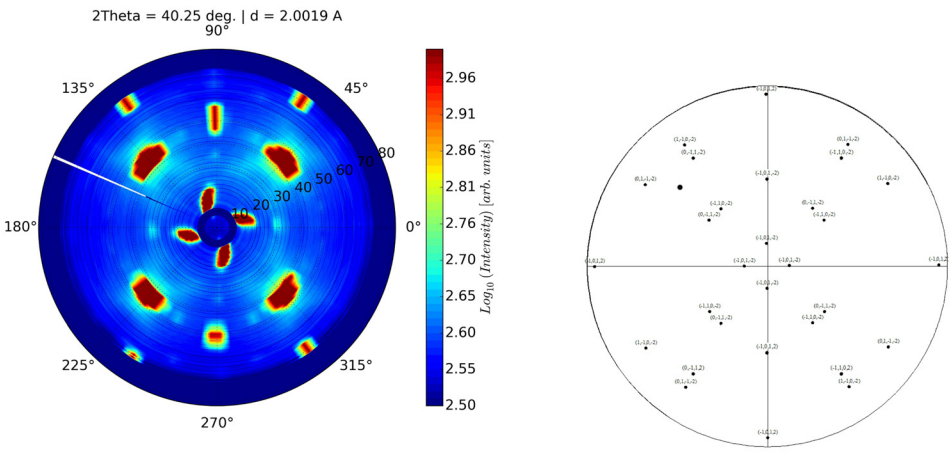

(a) (b)

FIG. 13. (a) Pole figure of the $\{10\bar{1}2\}$ planes of the intermetallic hexagonal phase measured after a 350 °C, (b) Corresponding stereographic projection.

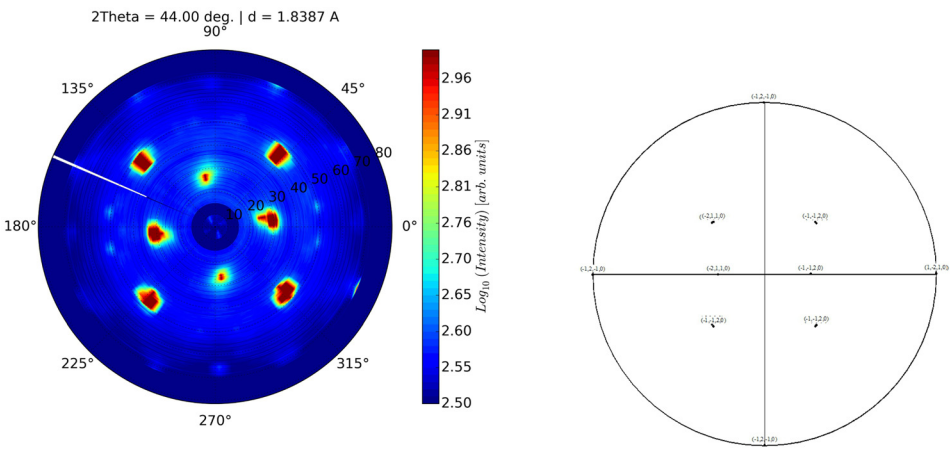

(a) (b)

FIG. 14. (a) Pole figure of the $\{11\bar{2}0\}$ planes of the intermetallic hexagonal phase measured after a 350 °C, (b) Corresponding stereographic projection. Extra poles on the pole figure correspond to the poles measured from the nearby {311} planes of the substrate.

Reuse of AIP Publishing content is subject to the terms at: https://publishing.aip.org/authors/rights-and-permissions. Download to IP: 132.168.90.240 On: Wed, 05 Oct 2016 07:24:46

Agency (ANR) under the "Investissements d'avenir" program (2 projects with the grant numbers: ANR-11-EQPX-0010 and FDSOI11) and within the framework of the Center of Excellence of Multifunctional Architectured Materials "CEMAM" No. AN-10-LABX-44-01 funded by the "Investments for the Future" Program. The authors would also thank Thierry Baron and his team from CNRS-LTM for the InGaAs epitaxy on InP.

APPENDIX A: POLE FIGURES OF THE INTERMETALLIC AFTER A 350 °C ANNEALING

Hereby, the pole figures of the $\{10\bar{1}1\}$, $\{10\bar{1}2\}$, and $\{11\bar{2}0\}$ planes (respectively, Figures 13(a) and 14(a)) of the intermetallic and their correspondent stereographic projection (respectively, Figures 13(b) and 14(b)).

APPENDIX B: POLE FIGURES OF THE $\{10\bar{1}1\}$ PLANES OF INTERMETALLIC AT DIFFERENT ANNEALING TEMPERATURES

Figures 15(a), 15(b), 15(c), and 15(d) show, respectively, the pole figures of the $\{10\bar{1}1\}$ planes measured after different RTA, at 300, 400, 450, and 550 °C on a Rigaku Smartlab using a Pilatus 100K area detector. The concentric circles on the pole figures do not have a significance and are the result of the superposition of different measurements at different χ angles.

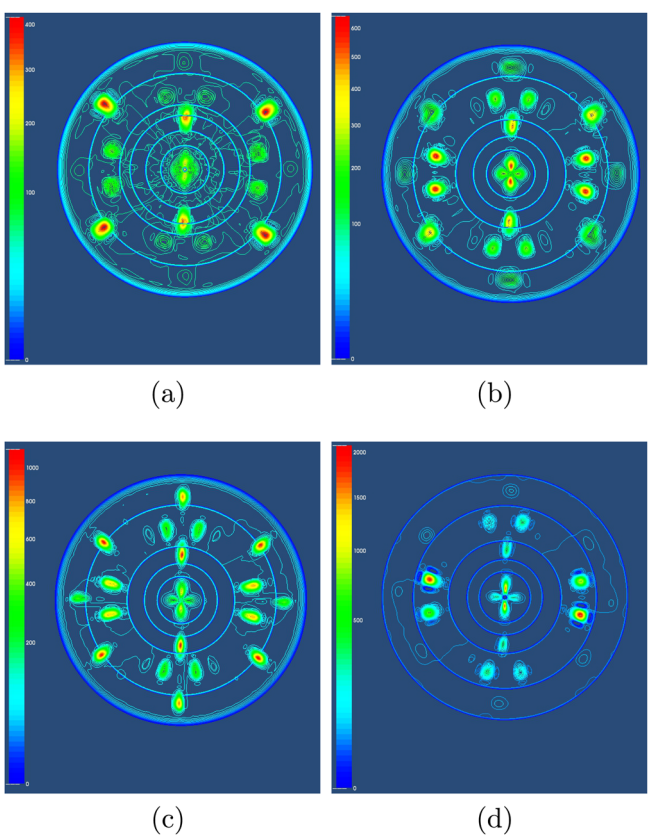

FIG. 15. Pole figure of the $\{10\bar{1}1\}$ planes of the intermetallic hexagonal phase measured after the following annealings: (a) 300 °C, (b) 400 °C, (c) 450 °C, (d) 550 °C.

[1]Linda Wilson, *International Technology Roadmap for Semiconductors* (Semiconductor Industry Association, 2013).
[2]J. A. del Alamo, "Nanometre-scale electronics with III–V compound semiconductors," Nature **479**, 317–323 (2011).
[3]H. Iwai, "Roadmap for 22 nm and beyond (Invited Paper)," Microelectron. Eng. **86**, 1520–1528 (2009).
[4]S. Gaudet, K. De Keyser, S. Lambert-Milot, J. Jordan-Sweet, C. Detavernier, C. Lavoie, and P. Desjardins, "Three dimensional reciprocal space measurement by x-ray diffraction using linear and area detectors: Applications to texture and defects determination in oriented thin films and nanoprecipitates," J. Vac. Sci. Technol., A **31**, 021505 (2013).
[5]C. Detavernier, A. S. Özcan, J. Jordan-Sweet, E. A. Stach, J. Tersoff, F. M. Ross, and C. Lavoie, "An off-normal fibre-like texture in thin films on single-crystal substrates," Nature **426**, 641–645 (2003).
[6]S. H. Kim, M. Yokoyama, N. Taoka, R. Iida, S. Lee, R. Nakane, Y. Urabe, N. Miyata, T. Yasuda, H. Yamada, N. Fukuhara, M. Hata, M. Takenaka, and S. Takagi, "Self-aligned metal source/drain $In_xGa_{1-x}As$ n-MOSFETs using Ni-InGaAs alloy," in *IEEE International Electron Devices Meeting (IEDM)*, San Francisco, CA, USA (2010), pp. 26.6.1–26.6.4.
[7]X. Zhang, H. Guo, X. Gong, Q. Zhou, Y.-R. Lin, H.-Y. Lin, C.-H. Ko, C. H. Wann, and Y.-C. Yeo, "$In_{0.7}Ga_{0.3}As$ channel n-MOSFET with self-aligned Ni-InGaAs source and drain," Electrochem. Solid-State Lett. **14**, H60–H62 (2011).
[8]A. Guivarc'h, R. Guérin, J. Caulet, A. Poudoulec, and J. Fontenille, "Metallurgical study of Ni/GaAs contacts. II. Interfacial reactions of Ni thin films on (111) and (001) GaAs," J. Appl. Phys. **66**, 2129–2136 (1989).
[9]A. Lahav, M. Eizenberg, and Y. Komem, "Interfacial reactions between Ni films and GaAs," J. Appl. Phys. **60**, 991–1001 (1986).
[10]Ivana, Y. Lim Foo, X. Zhang, Q. Zhou, J. Pan, E. Kong, M. H. Samuel Owen, and Y.-C. Yeo, "Crystal structure and epitaxial relationship of $Ni_4InGaAs_2$ films formed on InGaAs by annealing," J. Vac. Sci. Technol., B **31**, 012202 (2013).
[11]P. Shekhter, S. Mehari, D. Ritter, and M. Eizenberg, "Epitaxial NiInGaAs formed by solid state reaction on $In_{0.53}Ga_{0.47}As$: Structural and chemical study," J. Vac. Sci. Technol., B **31**, 031205 (2013).
[12]Ivana, J. Pan, Z. Zhang, X. Zhang, H. X. Guo, X. Gong, and Y.-C. Yeo, "Photoelectron spectroscopy study of band alignment at interface between Ni-InGaAs and $In_{0.53}Ga_{0.47}As$," Appl. Phys. Lett. **99**, 012105 (2011).
[13]X. Zhang, Ivana, H. X. Guo, X. Gong, Q. Zhou, and Y.-C. Yeo, "A self-aligned Ni-InGaAs contact technology for InGaAs channel n-MOSFETs," J. Electrochem. Soc. **159**, H511–H515 (2012).
[14]ICDD card No. 17-0881.
[15]S. Gaudet, C. Coia, P. Desjardins, and C. Lavoie, "Metastable phase formation during the reaction of Ni films with Si(001): The role of texture inheritance," J. Appl. Phys. **107**, 093515 (2010).
[16]C. Mocuta, M.-I. Richard, J. Fouet, S. Stanescu, A. Barbier, C. Guichet, O. Thomas, S. Hustache, A. V. Zozulya, and D. Thiaudière, "Fast pole figure acquisition using area detectors at the DiffAbs beamline–Synchrotron SOLEIL. Erratum," J. Appl. Crystallogr. **47**, 482 (2014).
[17]J.-F. Berar, N. Boudet, P. Breugnon, B. Caillot, B. Chantepie, J.-C. Clemens, P. Delpierre, B. Dinkespiller, S. Godiot, C. Meessen, M. Menouni, C. Morel, P. Pangaud, E. Vigeolas, S. Hustache, and K. Medjoubi, "{XPAD3} hybrid pixel detector applications," in *Radiation Imaging Detectors, 2008 Proceedings of the 10th International Workshop on Radiation Imaging Detectors* [Nucl. Instrum. Methods Phys. Res., Sect. A **607**, 233–235 (2009)].
[18]T. Thanh, N. Blanc, N. Boudet, E. Bourjot, S. Zhiou, V. Kovacova, P. Rodriguez, F. Nemouchi, and P. Gergaud, "Full 3d reciprocal space map of thin polycrystalline films for microelectronic applications," in *2015 IEEE International Interconnect Technology Conference and 2015 IEEE Materials for Advanced Metallization Conference (IITC/MAM)* (2015), pp. 53–56.
[19]C. Boudias and D. Monceau, *Carine Crystallography 3.1* (DIVERGENT SA, Centre de Transfert, 1989–1998).
[20]K. Momma and F. Izumi, "*VESTA3* for three-dimensional visualization of crystal, volumetric and morphology data," J. Appl. Crystallogr. **44**, 1272–1276 (2011).
[21]D. S. Covita, M. Ay, S. Schlesser, D. Gotta, L. M. Simons, E.-O. Le Bigot, and J. M. F. dos Santos, "Accurate miscut angle determination for spherically bent bragg crystals," Rev. Sci. Instrum. **79**, 033102 (2008).

Reuse of AIP Publishing content is subject to the terms at: https://publishing.aip.org/authors/rights-and-permissions. Download to IP: 132.168.90.240 On: Wed, 05 Oct 2016 07:24:46

[22]S. Lidin, "Superstructure ordering of intermetallics: B8 structures in the pseudo-cubic regime," Acta Crystallogr., Sect. B **54**, 97–108 (1998).
[23]T. Jarmar, J. Seger, F. Ericson, D. Mangelinck, U. Smith, and S.-L. Zhang, "Morphological and phase stability of nickelgermanosilicide on $Si_{1-x}Ge_x$ under thermal stress," J. Appl. Phys. **92**, 7193 (2002).
[24]S. Députier, A. Guivarc'h, J. Caulet, A. Poudoulec, B. Guenais, M. Minier, and R. Guérin, "Etude des interdiffusions en phase solide dans le contact Ni/AlAs," J. Phys. III **5**, 373–388 (1995).
[25]D. Hogan and D. Dyson, "Angles between planes in the hexagonal and tetragonal crystal systems," Micron **2**, 59–61 (1970).
[26]B. De Schutter, K. Van Stiphout, N. M. Santos, E. Bladt, J. Jordan-Sweet, S. Bals, C. Lavoie, C. M. Comrie, A. Vantomme, and C. Detavernier, "Phase formation and texture of thin nickel germanides on Ge(001) and Ge(111)," J. Appl. Phys. **119**, 135305 (2016).
[27]R. Chen and S. A. Dayeh, "Size and orientation effects on the kinetics and structure of nickelide contacts to InGaAs fin structures," Nano Lett. **15**, 3770–3779 (2015).
[28]R. Guérin and A. Guivarc'h, "Comment on Phase equilibria of the Ga–Ni–As ternary system [J. Appl. Phys. **80**, 543 (1996)]," J. Appl. Phys. **82**, 493 (1997).
[29]J. Philibert, F. M. d'Heurle, and P. Gas, "Diffusion-reaction: The ordered Cu_3Au rule and its corollaries," in *Diffusion and Reactions: From Basics to Applications*, Solid State Phenomena Vol 41 (Trans Tech Publications, 1995), pp. 93–102.

Reuse of AIP Publishing content is subject to the terms at: https://publishing.aip.org/authors/rights-and-permissions. Download to IP: 132.168.90.240 On: Wed, 05 Oct 2016 07:24:46